pp 271–290. © Royal Aeronautical Society 2016
doi: 10.1017/aer.2015.11

Effects of blade configuration parameters on helicopter rotor structural dynamics and whirl tower loads

M. Rohin Kumar
kumar.rohin@gmail.com

C. Venkatesan
Department of Aerospace Engineering
Indian Institute of Technology
Kanpur
India

ABSTRACT

The influence of the blade geometric parameters on the structural dynamic characteristics, response and loads of a helicopter rotor under hover condition in a whirl tower was investigated. A general geometry was considered for the rotor blade which included configuration parameters like root offset, torque offset, pre-twist, pre-cone, pre-droop, pre-sweep, tip-sweep and tip-anhedral. The option of placing concentrated masses at any location on the blade was also included. Natural frequencies and the corresponding mode shapes of the rotating blade were obtained by solving the linear, undamped structural dynamics model in the finite element domain. For calculating the response and loads on the rotor, the complete aeroelastic equation was solved in modal space. Aerodynamic models used in the aeroelastic loads calculations were Peters-He dynamic wake theory for inflow and the *modified* ONERA dynamic stall theory for airloads calculations. From the study, the blade structural dynamic characteristics are found to be sensitive to variation in blade geometric parameters. Tip-sweep was found to have significant effects on root oscillatory moments. The moments at the tip junction with the straight portion of the blade were found to be substantially affected by tip-sweep and tip-anhedral.

Keywords: Structural Dynamics; Rotor Loads; Rotary-wing Aeroelasticity

Received 22 January 2015; revised 13 July 2015; accepted 16 July 2015.

https://doi.org/10.1017/aer.2015.11 Published online by Cambridge University Press

NOMENCLATURE

a	torque offset or lift curve slope
c	blade chord ($= 2\ b$)
C_w	weight coefficient
e_1, e_2	root offset
$\{F_{AD}\}$	aerodynamic force vector
$[M]$	mass matrix or apparent mass matrix in inflow model
$[M^C]$	Coriolis damping matrix
N_b	number of blades in main rotor
O_H	hub centre
R	main rotor blade radius
β_d	blade pre-droop angle
β_p	blade pre-cone angle
β_s	blade pre-sweep angle
γ	lock number
Λ_a	tip-anhedral angle
Λ_s	tip-sweep angle
η, ζ	blade cross-sectional principal axes coordinates
θ_G	geometric pitch angle of rotor blade
θ_I	control pitch angle of rotor
θ_0	mean value of pitch angle or main rotor collective pitch angle
θ_{1c}, θ_{1s}	cyclic pitch angles for main rotor
ρ	density of air
σ	main rotor solidity ratio
ψ	azimuthal angle or non-dimensional time, Ωt

1.0 INTRODUCTION

The structural dynamics and aeroelastic characteristics of a rotor blade influence the performance of the helicopter in terms of loads, vibrations and handling qualities. These characteristics are sensitive to variations in blade geometric parameters[1]. There have been several studies reported in open literature which aimed to develop an understanding of the role played by these parameters in rotor loads and vibrations.

While it is known that pre-twist improves aerodynamic performance of the rotor blade, there have been differing observations on the influence of pre-twist on vibratory loads. In Ref. 2, it is shown that there is little sensitivity of blade vibration to pre-twist, while Refs 3 and 4 deduce that structural coupling from blade pre-twist significantly influences blade response and loads. In Ref. 4, it was also concluded that the magnitudes of oscillatory root and hub loads are significantly altered by variations in hinge- and root-offsets. In Ref. 5, it was shown that a 2.5° pre-cone angle resulted in reduced lead-lag bending loads as compared to those for a 2.5° droop.

Concentrated masses are added to the rotor blade for balancing. Ref. 3 showed that mass tuning is also effective in minimising vibratory hub loads. In Ref. 6, an optimisation procedure was developed to systematically place tuning masses along a rotor blade span to minimise vibratory loads. Ref. 7 concluded that the magnitude and location of the concentrated mass significantly influence the modal characteristics of the rotating beam.

https://doi.org/10.1017/aer.2015.11 Published online by Cambridge University Press

Tip-sweep and tip-anhedral are other important parameters used to improve rotor aerodynamic performance. In a recent study[8], the natural frequencies of a rotating beam with tip-sweep and tip-anhedral were obtained using a structural dynamic model and correlated with experimental data. With regards to vibration, both experimental[2] and analytical results[9,10] have shown reduction in 4/rev hub loads in forward flight with addition of tip-sweep. The study in Ref. 11 concluded that tip-sweep reduces flap and torsional oscillatory responses while tip-anhedral has considerable influence on flap dynamics.

In this article, the effects of blade geometry parameters are studied using an aeroelastic formulation of a generic rotor blade with non-linear structural and unsteady aerodynamic models. The objectives of this article are to determine:

(i) the effects of blade geometry parameters on rotating blade natural frequencies, and identify the parameters influencing the structural coupling in mode shapes

(ii) the effects of tip-sweep and tip-anhedral on loads at the blade root and also at the junction between the tip section and straight portion of the blade

2.0 BLADE STRUCTURAL MODEL

The rotor structural and aerodynamic models are described in detail in Ref. 12. For this work, a general geometry has been assumed for the rotor blade. Non-linearities in structural modelling and in aerodynamic modelling due to dynamic stall have been considered. An elastic rotating beam with constant angular velocity and features like blade root offset, torque offset, pre-twist, pre-cone, pre-droop, pre-sweep, tip-sweep and tip-anhedral was considered. The option of adding concentrated masses meant for blade tracking and balancing was also included. Figures 1(a) and 1(b) show the orthogonal co-ordinate systems describing the geometry of the rotating blade.

2.1 Co-ordinate transformations

In this section, the key co-ordinate transformations used in deriving the equations of motion of the rotor blade and involving the geometric features being studied are described. The relation between two orthogonal systems X_i, Y_i, Z_i and X_j, Y_j, Z_j with $\hat{e}_{xi}$, $\hat{e}_{yi}$ and $\hat{e}_{zi}$ and $\hat{e}_{xj}$, $\hat{e}_{yj}$ and $\hat{e}_{zj}$ as unit vectors along the respective axes can be written as:

$$\begin{Bmatrix} \hat{e}_{xi} \\ \hat{e}_{yi} \\ \hat{e}_{zi} \end{Bmatrix} = [T_{ij}] \begin{Bmatrix} \hat{e}_{xj} \\ \hat{e}_{yj} \\ \hat{e}_{zj} \end{Bmatrix} \quad \ldots (1)$$

where the transformation matrix $[T_{ij}]$ can be obtained using the Euler angles required to rotate the j-system so as to make it parallel to the i-system.

The angle between the $3K$ and $2K$ systems is $-\beta_p$ (Fig. 1(b)). Here, K refers to the kth blade. Applying the small-angle approximation ($\sin \beta_p \approx \beta_p$ and $\cos \beta_p \approx 1$), the transformation relation between these two systems is given by:

$$[T_{32}] = \begin{bmatrix} 1 & 0 & \beta_p \\ 0 & 1 & 0 \\ -\beta_p & 0 & 1 \end{bmatrix} \quad \ldots (2)$$

https://doi.org/10.1017/aer.2015.11 Published online by Cambridge University Press

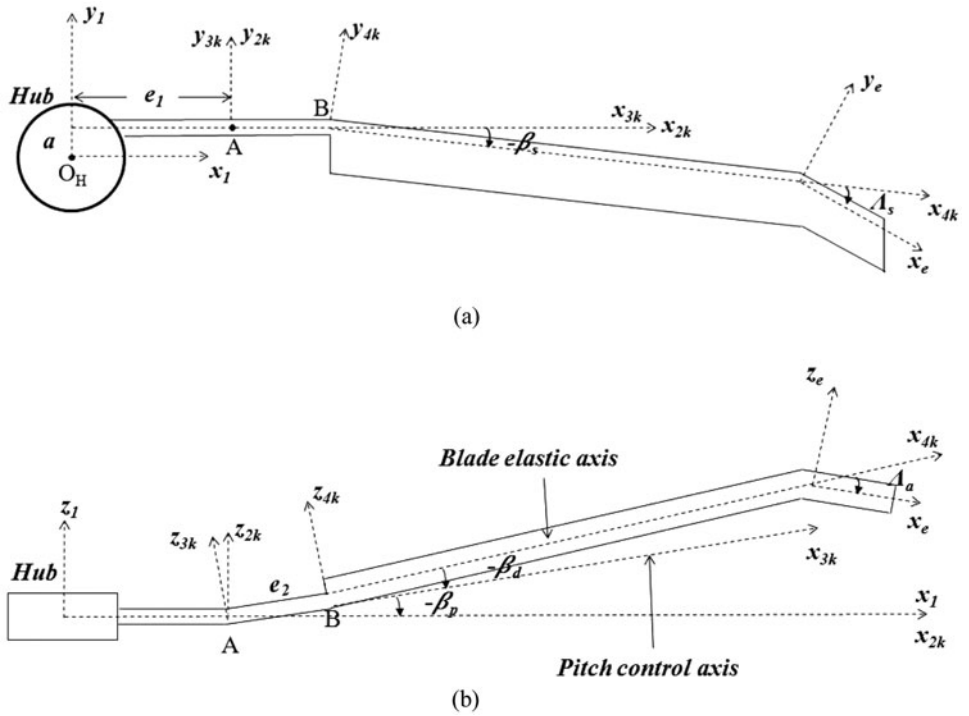


Figure 1. Blade co-ordinate systems: (a) blade top view and (b) blade front view.

The 4*K*-system is obtained by (i) translating the origin of the 3*K*-system by a distance 'e_2' along $\hat{e}_{x3k}$, (ii) then rotating the system by an angle $-\beta_s$ (pre-sweep angle) about z_{3k} axis, (iii) then rotating the system by an angle $-\beta_d$ (pre-droop angle) about y_{3k} axis, and finally, (iv) rotating the system by an angle θ_I (pitch input) about x_{3k} axis. The rotation sequence for obtaining the 4*K* system from the 3*K* system is a space-fixed rotation sequence[13], as all the rotations are about the 3*K*-axes. The transformation matrix, after applying small-angle approximation for angles β_s and β_d, is given by:

$$[T_{43}] = \begin{bmatrix} 1 & -(\beta_s \cos\theta_I + \beta_d \sin\theta_I) & (\beta_d \cos\theta_I - \beta_s \sin\theta_I) \\ \beta_s & \cos\theta_I & \sin\theta_I \\ -\beta_d & -\sin\theta_I & \cos\theta_I \end{bmatrix} \quad \ldots (3)$$

The transformation matrix between the *e*- and the 4*K* systems for the swept-tip element is given by:

$$[T_{e4}]_t = \begin{bmatrix} \cos\Lambda_s \cos\Lambda_a & -\sin\Lambda_s & \cos\Lambda_s \sin\Lambda_a \\ \sin\Lambda_s \cos\Lambda_a & \cos\Lambda_s & \sin\Lambda_s \sin\Lambda_a \\ -\sin\Lambda_a & 0 & \cos\Lambda_a \end{bmatrix} \quad \ldots (4)$$

where Λ_s is the blade tip sweep angle (positive for backward sweep) and Λ_a is the blade tip anhedral/dihedral angle (positive upward).

https://doi.org/10.1017/aer.2015.11 Published online by Cambridge University Press

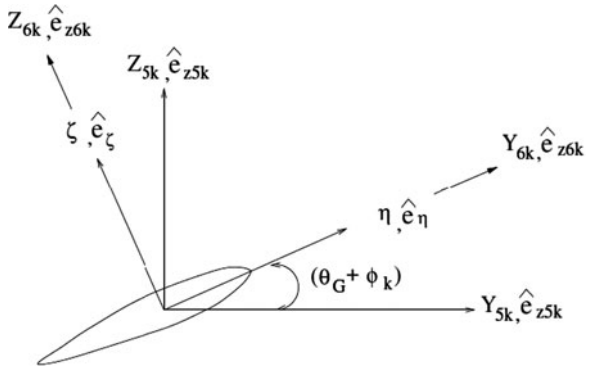


Figure 2. Cross-sectional principal co-ordinate system.

The 5*K*-system is the cross-sectional co-ordinate system of the *k*th blade. The 6*K*-system is obtained by rotating the 5*K*-system about $\hat{e}_{x5k}$ by an angle $(\phi_k + \theta_G)$, where θ_G is the geometric twist angle of the cross-section and ϕ_k is the elastic twist. The transformation relation between the 5*K*- and the 6*K*-systems (Fig. 2) is given by:

$$[T_{65}] = \begin{bmatrix} 1 & 0 & 0 \\ 0 & \cos(\phi_k + \theta_G) & \sin(\phi_k + \theta_G) \\ 0 & -\sin(\phi_k + \theta_G) & \cos(\phi_k + \theta_G) \end{bmatrix} \quad \ldots (5)$$

2.2 Equations of motion

The blade structural formulation follows the approach in Ref. 14. The non-linear equations of motion were derived for each beam element using Hamilton's principle. The equations are based on a moderate deflection theory and account for: arbitrary cross-sectional shape, pre-twist, generally anisotropic material behaviour, transverse shears and out-of-plane warping. Strain-displacement expressions are derived from Green's strain.

The blade is modelled by a series of straight beam finite elements along the elastic axis of the blade. Each beam element consists of two end nodes and one internal node at its mid-point, resulting in 14 degrees of freedom representing 4 lag, 4 flap, 3 torsional and 3 axial motion variables. Cubic Hermite interpolation polynomials are used for the bending displacement, while quadratic Lagrangian interpolation polynomials are used for torsional rotation and axial deflections.

2.3 Local-to-global co-ordinate transformation

Special care needs to be taken during assembly of the tip element matrices when tip-sweep or tip-anhedral is present. The local-to-global co-ordinate transformation for the tip element with sweep or anhedral can be written in the form

$$\boldsymbol{q}_t^L = [\Lambda]\,\boldsymbol{q}_t^G \quad \ldots (6)$$

where **q** represents the vector of unknown nodal degrees of freedom and the subscript *t* denotes quantities associated with the tip element; the superscripts *L* and *G* denote the local (*e*) and

https://doi.org/10.1017/aer.2015.11 Published online by Cambridge University Press

global ($4K$) co-ordinate system, respectively. The transformation matrix, $[\Lambda]$, is derived with the condition that the angular relationship between the tip-sweep (or tip-anhedral) and the straight portion of the blade at the junction is preserved after deformation[15]. The elements of the local-to-global transformation matrix $[\Lambda]$ for the tip element are given in the Appendix.

3.0 COMPLETE AEROELASTIC EQUATION FOR THE ROTOR BLADE

3.1 Structural dynamics analysis

The first step in the aeroelastic response study is to solve the linear, undamped structural dynamics model in the finite element domain to obtain the natural frequencies and the corresponding mode shapes of the rotating blade[16]. The governing equation for the ith finite element is

$$[M_i]\{\ddot{q}_i\} + [K_i]\{q_i\} = 0 \quad \ldots (7)$$

where $[M_i]$ represents the mass matrix of the ith element.

For cases with tip-sweep/anhedral, the governing equation for the tip element is given by

$$[\Lambda]^T [M_t][\Lambda]\{\ddot{q}_t\} + [\Lambda]^T [K_t][\Lambda]\{q_t\} = 0 \quad \ldots (8)$$

The element matrices are assembled to form the global finite element model for the rotor blade.

3.2 Aerodynamic model

The approach used for aerodynamic modelling has been described in detail in Refs 12 and 17. The aerodynamic model involves the evaluation of inflow (Peters-He model[18]), at various locations on the rotor disc and the evaluation of sectional aerodynamic loads (modified ONERA dynamic stall model[19]), on the rotor blade.

3.3 Aeroelastic equation

The global aeroelastic equation for the whole blade is obtained by assembling the elemental matrices from the kinetic and strain energy contributions,

$$[M]\{\ddot{\boldsymbol{q}}\} + [C]\{\dot{\boldsymbol{q}}\} + [K]\{\boldsymbol{q}\} = \{F_{AD}\} \quad \ldots (9)$$

where $\{F_{AD}\}$ is the aerodynamic force contribution. To reduce the number of degrees of freedom of the problem, modal co-ordinate transformation is performed on the aeroelastic equation. Eight modes comprising two lag, four flap, one torsion and one axial modes were used in the modal transformation. Solution of the non-linear aeroelastic equation of the main rotor involves successively calculating the inflow, rotor loads and the resulting response for a small time step. The time is then incremented and the calculation process is repeated until the converged periodic solution for a complete revolution is obtained. The flowchart of the solution procedure is shown in Fig. 3. The GSL math library[20] was used in the C++ program used to implement the algorithm. The models described in the previous sections and the solution procedure for loads and response calculations were validated for structural dynamics and whirl tower analysis in Ref. 12.

https://doi.org/10.1017/aer.2015.11 Published online by Cambridge University Press

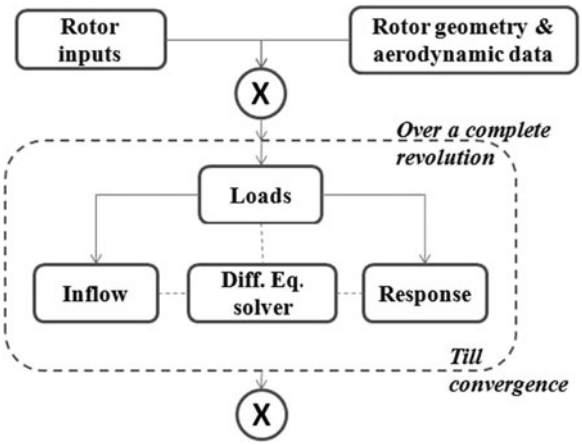


Figure 3. Flowchart for whirl tower analysis.

Table 1
Effect of torque- and hinge- offsets on natural frequencies (@ 314 RPM)

		Torque-offset(m)		Hinge-offset(m)	
Mode	**Baseline**	**0.05**	**0.1**	**0.05**	**0.1**
1st Lag	0.715	0.715	0.715	0.724	0.733
2nd Lag	5.306	5.306	5.306	5.322	5.339
1st Flap	1.098	1.098	1.098	1.103	1.108
2nd Flap	2.878	2.878	2.878	2.889	2.900
1st Torsion	4.377	4.377	4.377	4.377	4.378
1st Axial	33.342	33.342	33.342	33.342	33.342

4.0 EFFECTS OF BLADE CONFIGURATION PARAMETERS ON STRUCTURAL DYNAMICS

A parametric study was undertaken to study the effect of each of the various geometric parameters on the structural dynamic characteristics of the rotor blade. The baseline blade is an untwisted, straight blade with all geometric parameters (hinge-offset, torque-offset, pre-droop, pre-cone, pre-sweep, tip-sweep and tip-anhedral) set equal to zero. Each case consisted of setting a finite value to one geometric parameter at a time in the baseline blade. Blade mass distribution, m_0, was taken to be 8.45 kg/m and non-dimensional chord (c/R) was taken as 0.0757. The beam is clamped at the root.

4.1 Parametric study–results

4.1.1 Natural frequencies

Table 1 shows the effects of torque- and hinge-offsets on the natural frequencies of the blade. Torque-offset has no effect while the hinge-offset increases the bending frequencies. The torsional and axial frequencies are hardly affected.

https://doi.org/10.1017/aer.2015.11 Published online by Cambridge University Press

Table 2
Effect of pre-cone, pre-droop, pre-sweep on natural frequencies (@ 314 RPM)

		Pre-cone(deg)		Pre-droop(deg)		Pre-sweep(deg)	
Mode	**Baseline**	**2.5**	**5.0**	**2.5**	**5.0**	**2.5**	**5.0**
1st Lag	0.715	0.714	0.710	0.714	0.710	0.715	0.715
2nd Lag	5.306	5.306	5.305	5.306	5.305	5.306	5.306
1st Flap	1.098	1.098	1.095	1.098	1.095	1.098	1.098
2nd Flap	2.878	2.877	2.876	2.877	2.876	2.878	2.878
1st Torsion	4.377	4.377	4.377	4.377	4.377	4.377	4.377
1st Axial	33.342	33.342	33.342	33.342	33.342	33.342	33.342

Table 3
Effect of tip-sweep, tip-anhedral, tip-dihedral on natural frequencies (@ 314 RPM)

		Tip-sweep (deg)		Tip-anhedral (deg)		Tip-dihedral (deg)	
Mode	**Baseline**	**15**	**30**	**−10**	**−20**	**10**	**20**
1st Lag	0.715	0.716	0.717	0.715	0.714	0.715	0.714
2nd Lag	5.306	5.310	5.320	5.322	5.366	5.322	5.366
1st Flap	1.098	1.098	1.098	1.099	1.099	1.099	1.099
2nd Flap	2.878	2.876	2.872	2.879	2.881	2.879	2.881
1st Torsion	4.377	4.416	4.462	4.377	4.368	4.377	4.368
1st Axial	33.342	33.299	33.189	33.398	33.549	33.398	33.549

Table 2 shows the effect of pre-cone, pre-droop and pre-sweep on the natural frequencies. Pre-cone is the inclination of the pitch-change bearing with respect to the plane of rotation, while pre-droop is the inclination of the blade outboard of the pitch-change bearing. Both pre-cone and pre-droop slightly reduce the frequencies of the lower bending modes. The higher bending modes, torsional mode and axial mode, are hardly affected. Pre-droop has identical behaviour as pre-cone when both pitch input and pre-sweep angles are zero. This can be seen from their respective co-ordinate transformation matrices (Equations (2) and (3)). Pre-sweep does not have any effect on the frequencies.

Table 3 shows the effect of tip-geometry. The outboard 10% of the rotor blade is given a sweep or anhedral/dihedral angle. Tip-sweep is seen to increase the lag frequencies while flap frequencies are decreased. Tip-sweep effect is mostly seen in the torsional mode, the frequency of which is increased, while axial frequencies decrease with increase in tip-sweep. The reason for the increase in torsional frequency is the increase in torsional stiffness of the rotor blade due to the centrifugal force of the swept-tip. In the case of tip-anhedral (downward angle) and tip-dihedral (upward angle), both of which show the same effect, the bending (both lag and flap) and axial frequencies increase slightly, while the torsional frequency decreases with increase in tip-anhedral/dihedral.

https://doi.org/10.1017/aer.2015.11 Published online by Cambridge University Press

Table 4
Effects of concentrated mass radial location and magnitude (@ 314 RPM)

		1 kg			2 kg
Mode	**Baseline**	**0.5R**	**0.75R**	**1.0R**	**1.0R**
1st Lag	0.715	0.723	0.691	0.644	0.572
2nd Lag	5.306	5.265	5.318	5.148	5.013
1st Flap	1.098	1.101	1.085	1.066	1.035
2nd Flap	2.878	2.850	2.921	2.715	2.577
1st Torsion	4.377	4.377	4.377	4.377	4.377
1st Axial	33.342	33.041	32.744	32.633	31.951

Table 5
Effect of concentrated mass chordwise location (@ 314 RPM)

		1 kg tip mass @ 1.0R		
Mode	**Baseline**	**0.0m**	**−0.1m**	**0.1m**
1st Lag	0.715	0.644	0.644	0.644
2nd Lag	5.306	5.148	5.148	5.148
1st Flap	1.098	1.066	1.066	1.066
2nd Flap	2.878	2.715	2.714	2.714
1st Torsion	4.377	4.377	4.334	4.334
1st Axial	33.342	32.633	32.633	32.633

*Concentrated mass placed on elastic axis.

Concentrated masses are used in rotor blades for balancing and for reducing rotor vibration. They can also be in the form of sensors attached to the blade during experiments. Concentrated masses increase the modal mass of the rotor blade and also increase the centrifugal stiffening effect. Depending on the magnitude and the location of the mass, one of these effects is more dominant. When the modal mass increase is more dominant than the centrifugal stiffening effect, the natural frequency is reduced and vice-versa.

The effect of spanwise location and the effect of magnitude of concentrated mass is shown in Table 4. In general, as the spanwise location of the concentrated mass increases radially, the bending and axial frequencies decrease. The torsion frequency is left untouched as the mass is placed on the elastic axis. Increasing the magnitude of the concentrated mass (1 kg to 2 kg) reduces the bending and axial frequencies but does not affect the torsion mode. Table 5 shows the effect of chordwise location (from the elastic axis) of a tip mass. The torsional frequency reduces when the mass is moved away from the elastic axis. None of the other modes are affected.

The effect of pre-twist on the blade is shown in Table 6. The frequencies of the baseline untwisted blade are compared with those of blades having pre-twist of −12° and 12° such that the geometric twists at the section at $0.7R$ are zero. Airfoil portion of the blade begins at $0.25R$ and, hence, this is where pre-twist starts. The table shows that only the higher-bending

https://doi.org/10.1017/aer.2015.11 Published online by Cambridge University Press

Table 6
Effect of pre-twist (@ 314 RPM)

		Pre-twist	
Mode	**Baseline**	**−12°**	**12°**
1st Lag	0.715	0.715	0.715
2nd Lag	5.306	5.296	5.296
1st Flap	1.098	1.098	1.098
2nd Flap	2.878	2.879	2.879
1st Torsion	4.377	4.376	4.376
1st Axial	33.342	33.342	33.342

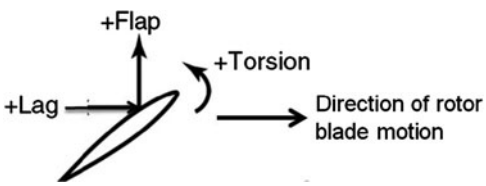


Figure 4. Positive directions for the airfoil degrees of freedom.

(lag and flap) frequencies are slightly affected due to the pre-twist. There is hardly any change in the frequency of the torsional mode. Pre-twist does not have much effect on the natural frequencies because the neck region of the blade ($<0.25R$) with less stiffness than the airfoil region primarily determines the structural dynamics characteristics.

Summarising from the results above, of all the geometric parameters, hinge-offset affects the bending (lag and flap) frequencies the most without affecting the torsion frequency. Tip-sweep affects torsion frequency the most with least effect on the bending frequencies. Torsion frequency can also be altered without affecting the bending frequencies by placing concentrated masses with a chord-offset.

4.1.2 Mode shapes

Next, the effects of the geometric parameters on mode shapes are studied. Changes in mode shapes alter the modal generalised forces. In this section, only those cases which show some effect on the mode shapes have been plotted. Only the first lag and first flap modes are plotted. The sign convention for the mode shapes are shown in Fig. 4. It is to be noted that pitch-up deformation is taken as positive. Figures 5-9 show the first lag and first flap modes along with the corresponding coupled torsion or axial deformation for the cases of pre-cone, tip-sweep, tip-anhedral and pre-twist. The other geometric parameters were found to have negligible influence as far as the mode shapes are concerned.

Figure 5(a) shows the first lag mode for the baseline blade. It was observed that there is no change in the mode shape with inclusion of pre-cone angle. Hence, for legibility, only the baseline blade mode shape has been plotted here. Figure 5(b) shows the participation of torsion deformation in this mode. It can be seen that while the lag mode shape is not significantly affected by pre-cone, the coupled torsion deformations have been substantially affected. There is an increasing pitch-up deformation with increase in pre-cone. Similarly,

https://doi.org/10.1017/aer.2015.11 Published online by Cambridge University Press

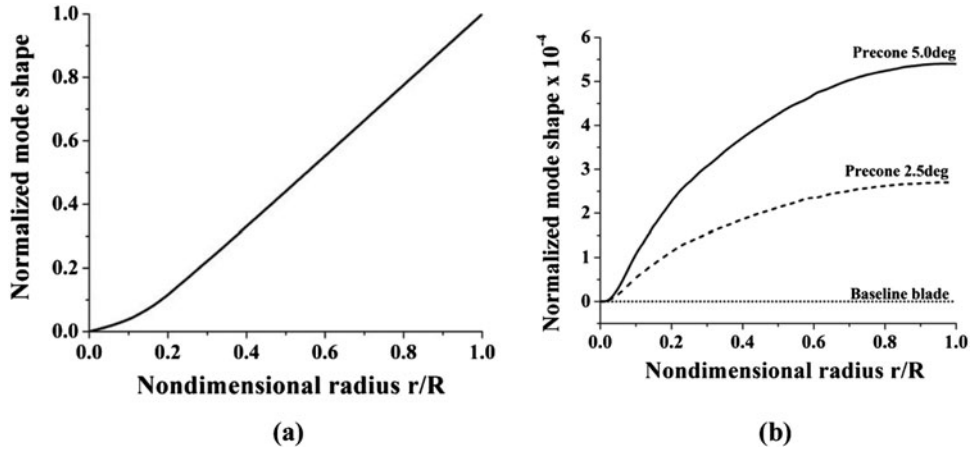


Figure 5. Effect of pre-cone on 1st lag mode. (a) 1st Lag. (b) Torsion participation in 1st Lag.

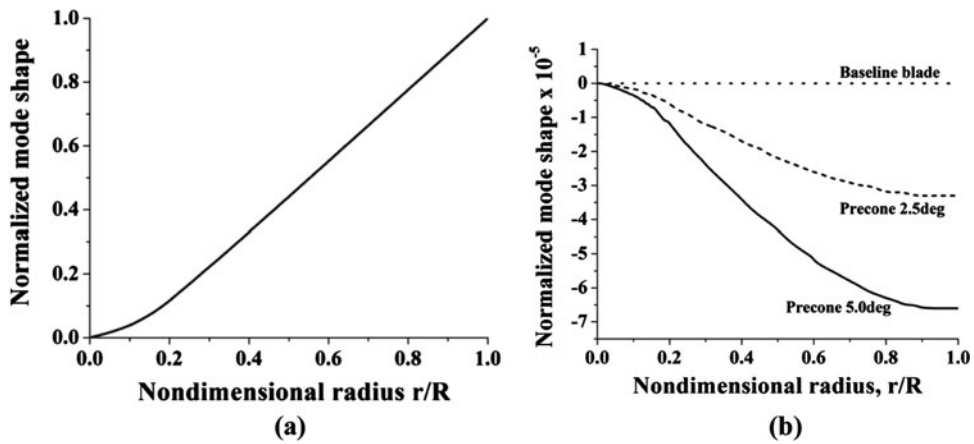


Figure 6. Effect of pre-cone on 1st flap mode. (a) 1st Flap (b) Axial participation in 1st Flap.

Fig. 6(a) shows the first flap mode of the baseline blade. There is no change in this mode with increase in pre-cone angle. The first flap mode was found to be coupled with axial mode and this can be seen in Fig. 6(b). The participation of the axial deformation in this mode is observed to be increasing with increase in the pre-cone angle.

Figures 7 and 8 show the effect of tip-sweep and tip-anhedral/dihedral on the mode shapes. Tip-sweep was found to induce flap-torsion coupling, while tip-anhedral/dihedral was found to induce lag-torsion coupling. This can be explained by the fact that there is an in-plane offset of the centre of gravity at the tip in the case of tip-sweep which causes a pitching moment about the elastic axis during flap motion. Similarly, there is an out-of-plane offset of the centre of gravity at the tip in the case of tip-anhedral which causes a pitching moment about the elastic axis during lead-lag motion. The torsion participation in the first flap mode with increase in tip-sweep is shown in Fig. 7(b). There is no effect of tip-sweep on the flap mode (Fig. 7(a)) itself and hence, only the baseline blade flap mode is shown. Only the coupled torsion deformation is affected by tip-sweep, and it is seen that there is an increasingly pitch-down

https://doi.org/10.1017/aer.2015.11 Published online by Cambridge University Press

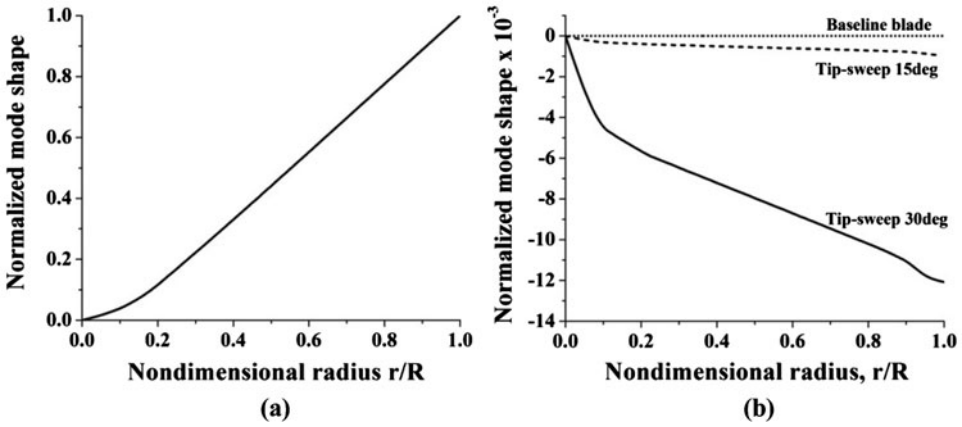


Figure 7. Effect of tip-sweep on mode shapes. (a) 1st Flap (b) Torsion participation in 1st Flap.

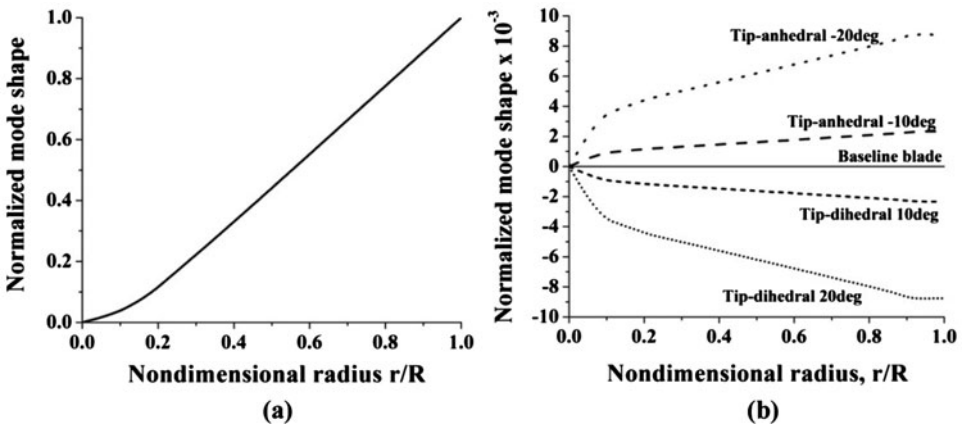


Figure 8. Effect of Tip-anhedral/dihedral on mode shapes. (a) 1st Lag (b) Torsion participation in 1st Lag.

deformation with increase in sweep. Similarly, in Fig. 8(b), it is seen that the coupled torsion deformation in first lag is pitch-up for tip-anhedral case and pitch-down for tip-dihedral case. The torsion participation is seen to increase with increase in tip-anhedral/dihedral. There is no effect of tip-anhedral on the lag mode (Fig. 8(a)).

Pre-twist in rotor blades causes coupling of flap and lead-lag motion. This can be seen from Fig. 9 where the mode shapes of the baseline untwisted blade are compared with those of blades having pre-twist of $-12°$ and $12°$, such that the geometric pitch angle at the section at $0.7R$ are zero. Figure 9(b) shows flap participation in first lag mode and Fig. 9(d) shows lag participation in the first flap mode. The positive and negative twists produce opposite effects in the coupled motion as seen in the figures. However, there is no effect of pre-twist on the bending modes themselves (Fig. 9(a) for first lag and Fig. 9(c) for first flap). There is no change in the mode shape of the torsional mode due to the blade pre-twist and hence, the torsional mode has not been plotted.

https://doi.org/10.1017/aer.2015.11 Published online by Cambridge University Press

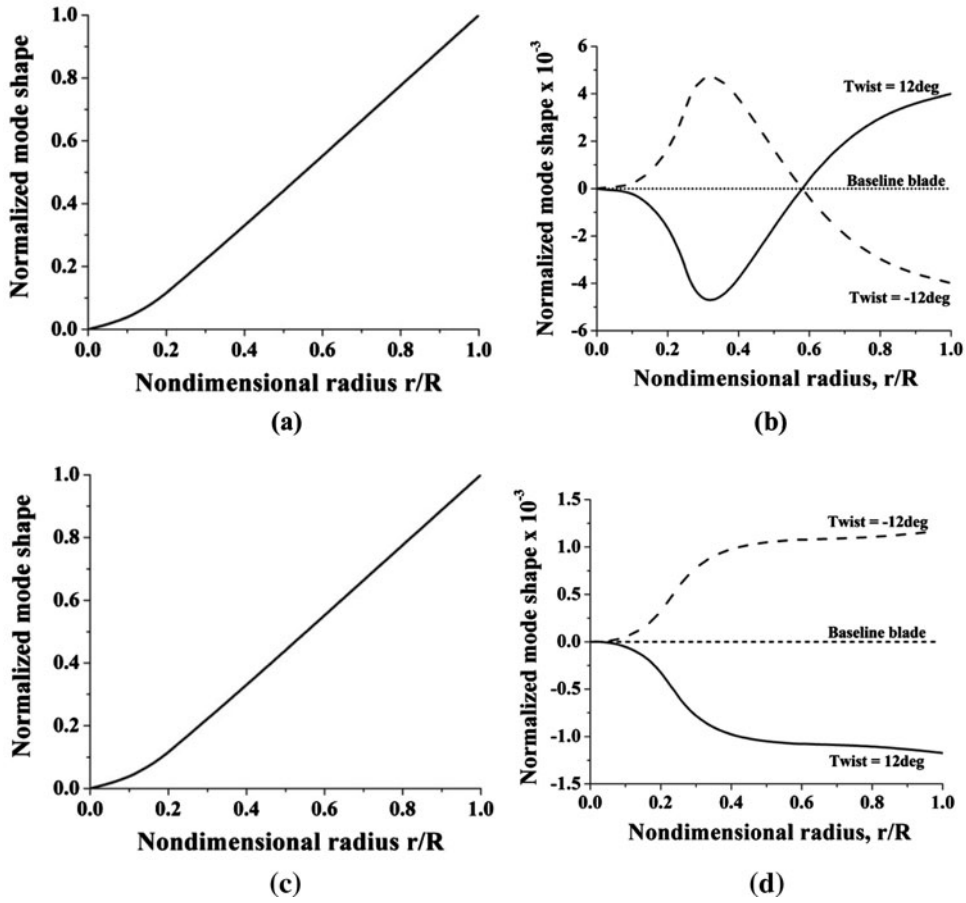


Figure 9. Effect of pre-twist on mode shapes. (a) 1st Lag (b) Flap participation in 1st Lag. (c) 1st Flap (d) Lag participation in 1st Flap.

5.0 EFFECTS OF BLADE CONFIGURATION PARAMETERS ON WHIRL TOWER LOADS

5.1 Effects of collective input

In a whirl tower, the rotor is mounted above the ground on a vertical stand with a motor with facility to change rotor collective and cyclic pitch input. The general effects of the blade configuration parameters on the whirl tower loads with variation in collective angle have been studied in Ref. 12. The geometry of the rotor of the whirl tower used for the analysis is given in Table 7. It was seen in this study that pre-cone and pre-droop reduce root flap bending stresses at higher collective angles. Similarly, torque offset was seen to reduce the root lead-lag moment. The other parameters were found not to have significant effects on the root moments and tip displacements. However, tip geometry effects were not considered in this reference.

Figure 10 shows the effects of tip-sweep and tip-anhedral with change only in collective angle. It is seen that these two parameters do not have much effect on thrust and power coefficients (Figs 10(a), 10(b)), and the root bending moments (Figs 10(c), 10(d)). However, it

https://doi.org/10.1017/aer.2015.11 Published online by Cambridge University Press

Table 7
Rotor data

Parameters		Value
Number of blades	N_b	4
Air density at sea level	ρ (kg/m^3)	1.224
Blade mass distribution	m_0 (kg/m)	8.45
Blade chord	c (m)	0.5
Rotor radius	R (m)	6.6
Solidity ratio	Σ	0.09646
Weight coefficient	C_w	0.00734
Lift-curve slope	$C_{l\alpha}$	5.73
Profile drag coefficient	C_{d0}	0.01
Lock number	Γ	6.4
RPM	Ω	314

is interesting to note that tip-sweep induces a large increase in the lag moment at 0.9R which is its junction with the straight portion of the blade (Fig. 10(e)). Similarly, tip-anhedral causes an increase in flap moment at 0.9R (Fig. 10(f)).

5.2 *Effects of cyclic input along with collective*

Giving only a collective input produces only non-oscillatory loads in the whirl tower blades. Oscillatory loads are generated in the whirl tower blades when cyclic inputs are introduced. In this section, the effects of tip-sweep and tip-anhedral on the blade oscillatory loads due to a 2° lateral cyclic input along with a 5° collective are studied. It is necessary to give a minimum collective angle so that the system has sufficient aerodynamic damping in flap.

Figure 11 shows the effects of tip-sweep on blade response @ 0.7R and the root blade moments. The lag response and root lag moment show a slight reduction in peak-to-peak values for a small tip-sweep angle (5°); but at higher tip-sweep (15°), the peak-to-peak values show an increase. Flap response and root flap moment are hardly affected by tip-sweep and hence, have not been plotted. The torsion response is seen to decrease with increase in tip-sweep. This is due to the inertia of the tip portion providing a pitch-up moment to the blade. The root pitch-down moment is seen to increase in magnitude with increase in tip-sweep. Figure 12 shows the pitching and lag moments at the junction between the tip-sweep and straight portion of the blade. It is seen that tip-sweep increases these moments at the junction substantially.

Figure 13 shows the effects of tip-anhedral on blade response @ 0.7R and the root blade moments. The lag response and root lag moment are hardly affected. The flap response and root flap moment also have negligible effects and hence, are not shown here. The most noticeable effect of tip-anhedral is the reduction in the torsion response. Figure 14 shows the pitching and flap moments at the junction between the tip-anhedral and straight portion of the blade. Just as in the case with only collective input, the flap moment is seen to be affected by tip-anhedral/dihedral. Tip-anhedral increased the negative flap moment while tip-dihedral has decreased it.

https://doi.org/10.1017/aer.2015.11 Published online by Cambridge University Press

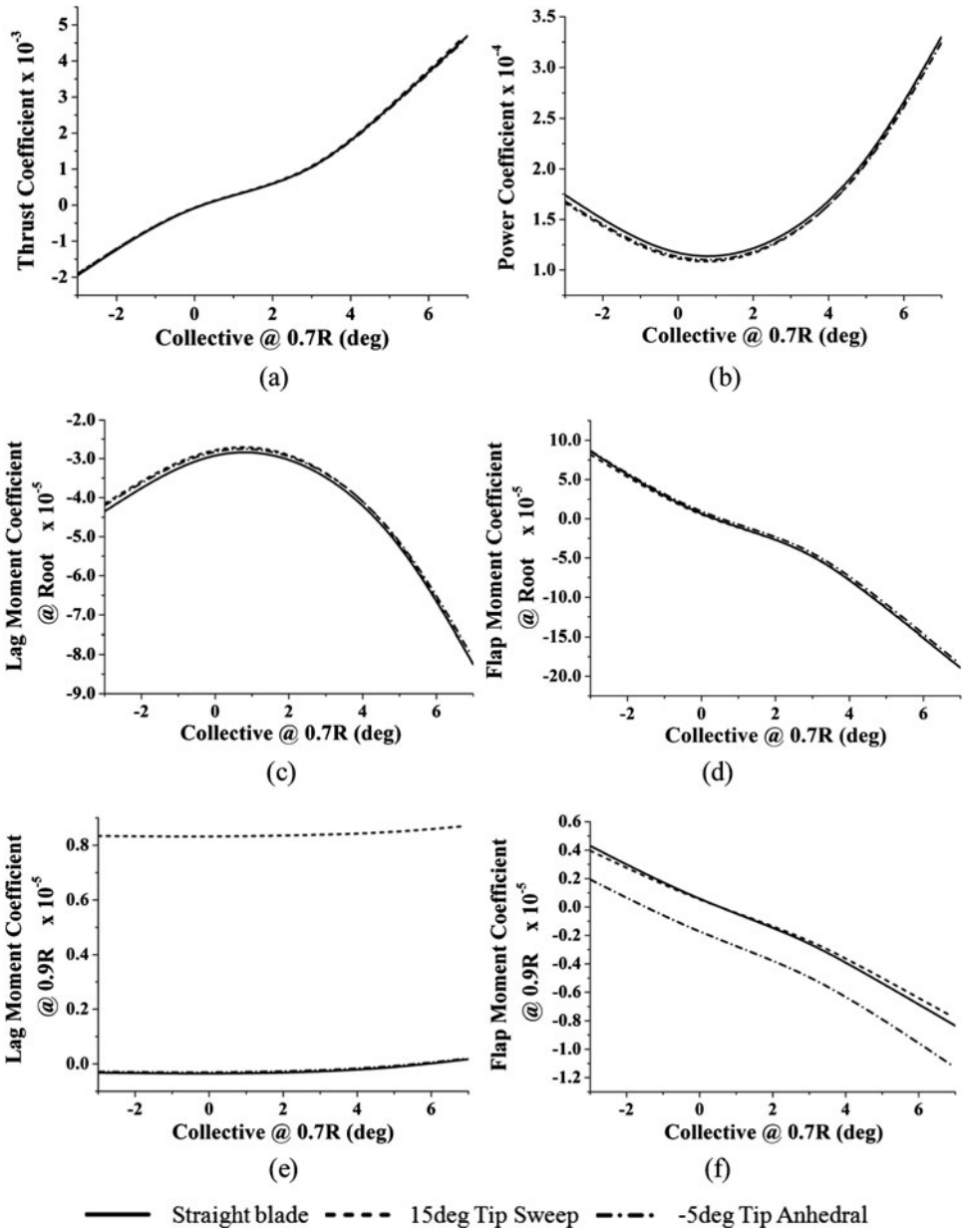


Figure 10. Variation of effects of tip sweep and tip anhedral with only collective input.

6.0 CONCLUDING REMARKS

The influence of the blade geometric parameters on the structural dynamic characteristics, and response and loads of the rotor in a whirl tower simulation was studied. The key observations from this investigation are:

https://doi.org/10.1017/aer.2015.11 Published online by Cambridge University Press

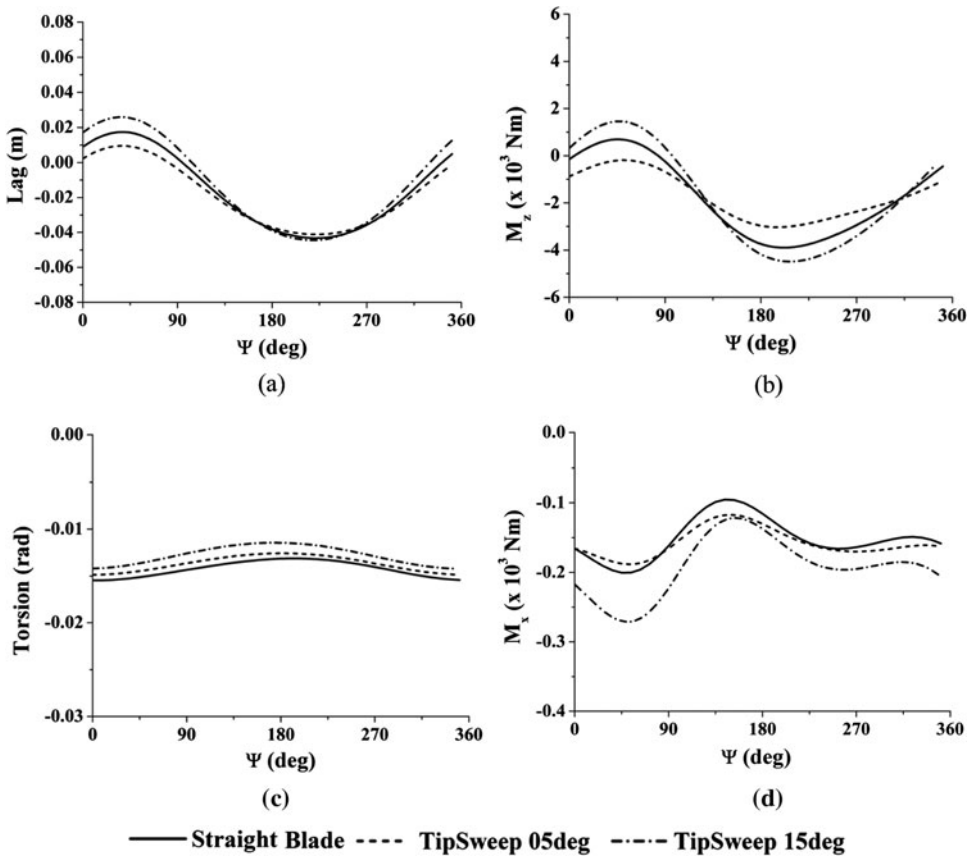


Figure 11. Effect of tip-sweep on blade responses @ 0.7*R* and blade root moments with 2° lateral cyclic input and 5° collective. (a) Lag @0.7*R* (b) Root Lag Moment. (c) Torsion @0.7*R* (d) Root Pitching Moment.

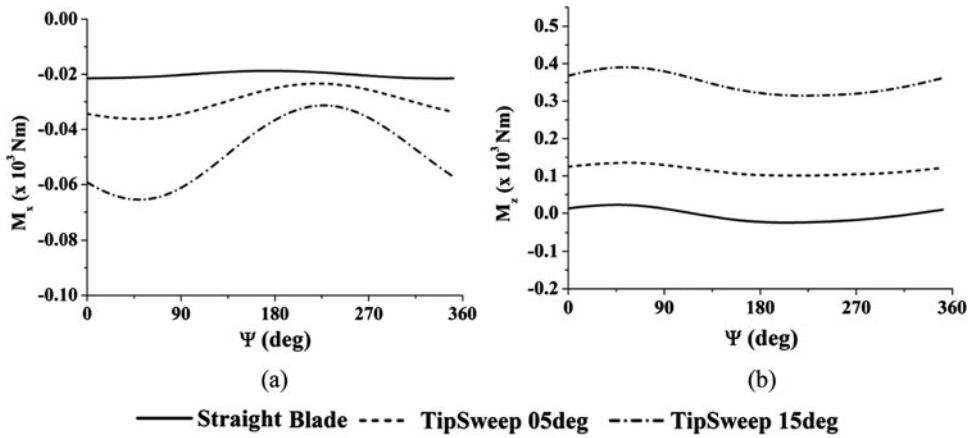


Figure 12. Bending moments @0.9*R* for tip-sweep. (a) pitching moment (b) lag moment.

https://doi.org/10.1017/aer.2015.11 Published online by Cambridge University Press

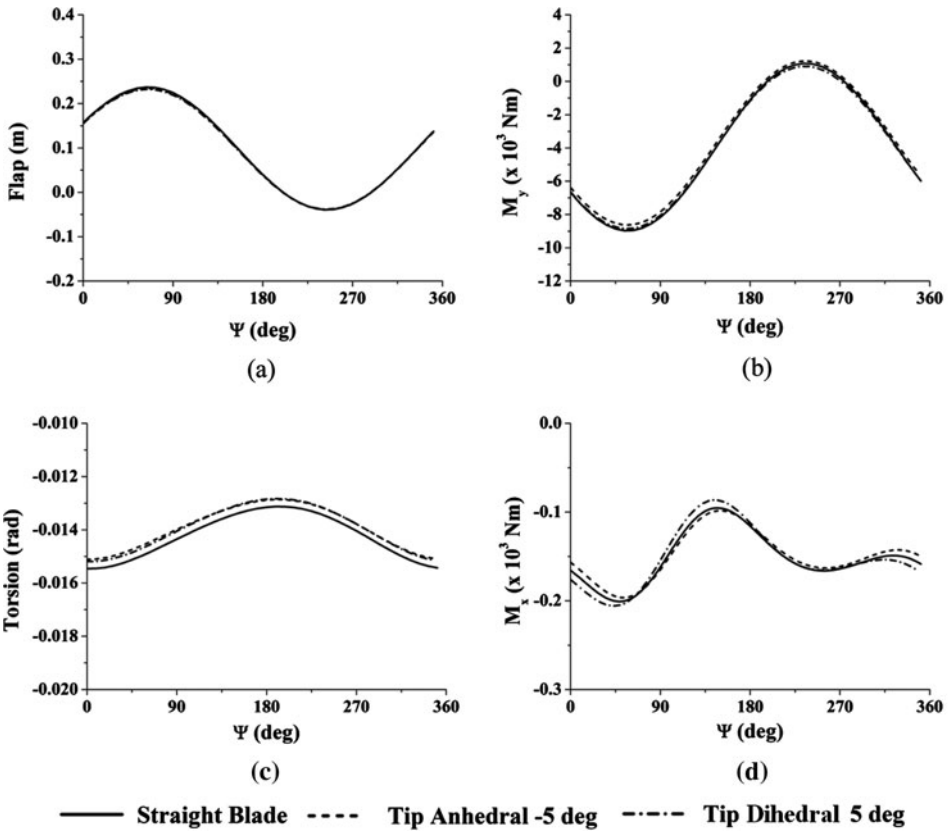


Figure 13. Effect of tip-anhedral on blade response @ 0.7*R* and on blade root moments with 5° collective and 2° lateral cyclic input. (a) Flap @0.7*R* (b) root flap moment. (c) Torsion @0.7*R* (d) root pitching moment.

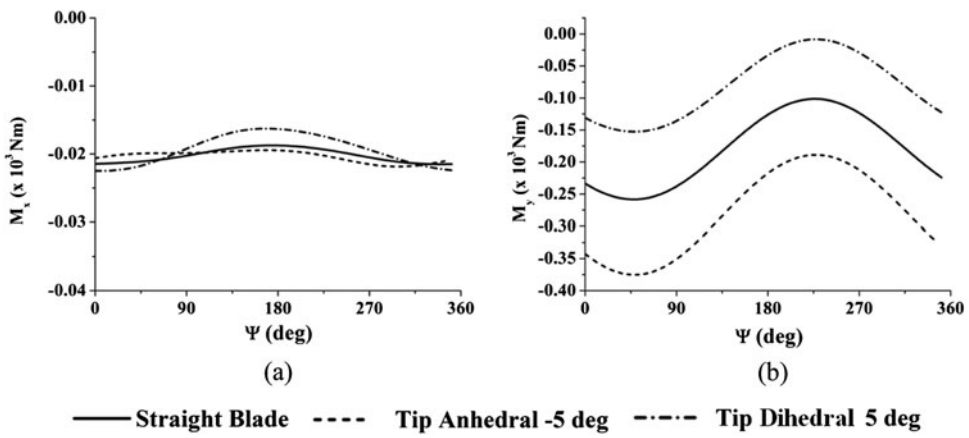


Figure 14. Bending moments @0.9*R* for tip-anhedral. (a) pitching moment (b) flap moment.

https://doi.org/10.1017/aer.2015.11 Published online by Cambridge University Press

- The bending (lag and flap) frequencies can be tuned without affecting the torsion frequency by varying the hinge-offset.
- The torsion frequency can be tuned with least effect on the bending frequencies by varying tip-sweep and chord-wise placement of concentrated mass.
- As the span-wise location of a concentrated mass moves towards the blade tip, the first flap and lag frequencies are reduced.
- The second flap and lag frequencies initially increase and then decrease as a concentrated mass is moved towards the tip. The reason for this behaviour is a node observed near $0.75R$ in the mode shape. For a concentrated mass placed at a node, inertia effect is reduced but centrifugal effect is preserved.

In the whirl tower simulation, a cyclic pitch input was provided in addition to a collective pitch angle in order to generate oscillatory response and loads on the blade. From this study, it is observed that

- Tip-sweep increases the oscillatory lag moment at the blade root.
- Both tip-sweep and tip-anhedral decrease the elastic torsion deformation of the blade. However, the root pitching moment is significantly increased, especially, due to tip-sweep.
- Tip-sweep and tip-anhedral are found to alter the bending moments at the junction between the straight portion of the blade and the tip element. In particular, tip-sweep increases the lag bending moment while tip-anhedral increases the flap bending moment at the junction, substantially.

ACKNOWLEDGEMENTS

The authors thank Hindustan Aeronautics Limited, Bangalore, India for providing the financial support for this research work.

APPENDIX

The non-zero elements of the local-to-global transformation matrix, $[\Lambda]$, for a tip element with tip-sweep and tip-anhedral are given here (Section 2.3):

$\Lambda\,[1, 1] = \cos\Lambda_s$

$\Lambda\,[1, 3] = \sin\Lambda_s \sin\Lambda_a$

$\Lambda\,[1, 6] = \sin\Lambda_s \cos\Lambda_a$

$\Lambda\,[2, 2] = \cos\Lambda_a$

$\Lambda\,[2, 5] = -\sin\Lambda_a$

$\Lambda\,[3, 3] = \cos\Lambda_a$

$\Lambda\,[3, 6] = -\sin\Lambda_a$

$\Lambda\,[4, 2] = \sin\Lambda_s \sin\Lambda_a$

$\Lambda\,[4, 4] = \cos\Lambda_s$

$\Lambda\,[4, 5] = \sin\Lambda_s \cos\Lambda_a$

$\Lambda\,[5, 2] = \cos\Lambda_s \sin\Lambda_a$

https://doi.org/10.1017/aer.2015.11 Published online by Cambridge University Press

$\Lambda\ [5, 4] = -\sin\Lambda_s$
$\Lambda\ [5, 5] = \cos\Lambda_s \cos\Lambda_a$
$\Lambda\ [6, 1] = -\sin\Lambda_s$
$\Lambda\ [6, 3] = \cos\Lambda_s \sin\Lambda_a$
$\Lambda\ [6, 6] = \cos\Lambda_s \cos\Lambda_a$
$\Lambda\ [7, 2] = 1/2 \cos\Lambda_s \sin\Lambda_a$
$\Lambda\ [7, 4] = -1/2 \sin\Lambda_s$
$\Lambda\ [7, 7] = \cos\Lambda_s \cos\Lambda_a$
$\Lambda\ [7, 10] = 1/2 \cos\Lambda_s \sin\Lambda_a$
$\Lambda\ [7, 12] = -1/2 \sin\Lambda_s$
$\Lambda\ [8, 1] = -1/2 \sin\Lambda_s$
$\Lambda\ [8, 3] = 1/2 \cos\Lambda_s \sin\Lambda_a$
$\Lambda\ [8, 8] = \cos\Lambda_s \cos\Lambda_a$
$\Lambda\ [8, 9] = -1/2 \sin\Lambda_s$
$\Lambda\ [8, 11] = 1/2 \cos\Lambda_s \sin\Lambda_a$
$\Lambda\ [9, 9] = \cos\Lambda_s$
$\Lambda\ [9, 11] = \sin\Lambda_s \sin\Lambda_a$
$\Lambda\ [9, 14] = \sin\Lambda_s \cos\Lambda_a$
$\Lambda\ [10, 10] = \cos\Lambda_a$
$\Lambda\ [10, 13] = -\sin\Lambda_a$
$\Lambda\ [11, 11] = \cos\Lambda_a$
$\Lambda\ [11, 14] = -\sin\Lambda_a$
$\Lambda\ [12, 10] = \sin\Lambda_s \sin\Lambda_a$
$\Lambda\ [12, 12] = \cos\Lambda_s$
$\Lambda\ [12, 13] = \sin\Lambda_s \cos\Lambda_a$
$\Lambda\ [13, 10] = \cos\Lambda_s \sin\Lambda_a$
$\Lambda\ [13, 12] = -\sin\Lambda_s$
$\Lambda\ [13, 13] = \cos\Lambda_s \cos\Lambda_a$
$\Lambda\ [14, 9] = -\sin\Lambda_s$
$\Lambda\ [14, 11] = \cos\Lambda_s \sin\Lambda_a$
$\Lambda\ [14, 14] = \cos\Lambda_s \cos\Lambda_a$

REFERENCES

1. GUPTA, B.P. Blade Design Parameters which Affect Helicopter Vibrations. In *Proceedings of the 40th AHS Annual Forum*, 1984, Washington, DC, US.
2. BLACKWELL, R.H. Blade design for reduced helicopter vibration. *J Am Helicopter Soc*, 1983, **28**, (3), pp 33-41.
3. HE, C. A parametric study of harmonic rotor hub loads. NASA Contractor Report 4558, 1993.
4. LAXMAN, V., VENKATESAN, C. and BYUN, Y.H. Influence of blade geometric parameters on aeroelastic response of a helicopter rotor system. *J Aerospace Eng*, 2011, **26**, (3), pp 555-570.
5. GÖTZFRIED, K. Survey of Tiger main rotor loads from design to flight test. *J Am Helicopter Soc*, 2002, **47**, (4), pp 285-296.

https://doi.org/10.1017/aer.2015.11 Published online by Cambridge University Press

6. PRITCHARD, J.I., ADELMAN, H.M., WALSH, J.L. and WILBUR, M.L. Optimizing tuning masses for helicopter rotor blade vibration reduction and comparison with test data. *J Aircraft*, 1993, **30**, (6), pp 906-910.
7. YOO, H.H., SEO, S. and HUH, K. The effect of a concentrated mass on the modal characteristics of a rotating cantilever beam. *Proc Inst Mech Eng C*, 2002, **216**, (2), pp 151-163.
8. PICCIONE, E., BERNARDINI, G. and GENNARETTI, M. Structural aeroelastic finite element modeling for advanced-geometry rotor blades. *Aircraft Eng Aerospace Technol*, 2012, **84**, (6), pp 367-375.
9. YEN, J.G. Effects of blade tip shape on dynamics, cost, weight, aerodynamic performance, and aeroelastic response. *J Am Helicopter Soc*, 1994, **39**, (4), pp 37-45.
10. CELI, R. and FRIEDMANN, P. Structural optimization with aeroelastic constraints of rotor blades with straight and swept tips. *AIAA J*, 1990, **28**, (5), pp 928-936.
11. KIM, K.C. and CHOPRA, I. Aeroelastic analysis of swept, anhedral, and tapered tip rotor blades. *J Am Helicopter Soc*, 1992, **37**, (1), pp 15-30.
12. KUMAR, R. and VENKATESAN, C. Rotorcraft aeroelastic analysis using dynamic wake/dynamic stall models and its validation. *J Aeroelasticity Struct Dyn*, 2013, **3**, (1), pp 65-87.
13. GINSBERG, J. *Engineering Dynamics*, 2008, **10**. Cambridge University Press.
14. YUAN, K.A., VENKATESAN, C. and FRIEDMANN, P.P. A new aeroelastic model for composite rotor blades with straight and swept tips. In *33rd AIAA Structural Dynamics and Materials Conference*, AIAA 92-2259. April 1992, Dallas, Texas, US.
15. PANDA, B. Technical note: Assembly of moderate-rotation finite elements used in helicopter rotor dynamics. *J Am Helicopter Soc*, 1987, **32**, (4), pp 63-69.
16. YUAN, K.A., VENKATESAN, C. and FRIEDMANN, P.P. Structural dynamic model of composite rotor blades undergoing moderate deflections. In Recent Advances in the Structural Dynamic Modelling of Composite Rotor Blades and Thick Composites, ASME Ad-Vol. 30, Winter Annual Meeting of ASME Anaheim. November 1992, California, US.
17. LAXMAN, V. and VENKATESAN, C. Chaotic response of an airfoil due to aeroelastic coupling and dynamic stall. *AIAA J*, 2007, **45**, (1), pp 271-280.
18. HE, C. *Development and Application of a Generalized Dynamic Wake Theory for Lifting Rotors*. PhD thesis, Georgia Institute of Technology, July 1989, Atlanta, GA, US.
19. PETOT, D. Differential equation modeling of dynamic stall. *La Reserche Aerospatiale*, (1989-5), pp 59-72.
20. GSL - GNU scientific library. http://www.gnu.org/software/gsl/.

https://doi.org/10.1017/aer.2015.11 Published online by Cambridge University Press